Characterization of Neodymium Calcium Oxyborate Piezoelectric Crystals With Monoclinic Phase

ARTICLE *in* CRYSTAL GROWTH & DESIGN · MARCH 2010

Impact Factor: 4.89 · DOI: 10.1021/cg9015756

6 AUTHORS, INCLUDING:

Fapeng Yu
Shandong University
71 PUBLICATIONS **575** CITATIONS
SEE PROFILE

Shujun Zhang
Pennsylvania State University
403 PUBLICATIONS **7,299** CITATIONS
SEE PROFILE

Xian Zhao
Shandong University
229 PUBLICATIONS **2,005** CITATIONS
SEE PROFILE

Chun-Ming Wang
Shandong University
83 PUBLICATIONS **1,014** CITATIONS
SEE PROFILE

DOI: 10.1021/cg9015756

CRYSTAL GROWTH & DESIGN Article

2010, Vol. 10
1871–1877

Characterization of Neodymium Calcium Oxyborate Piezoelectric Crystal with Monoclinic Phase

Fapeng Yu,[†,‡] Shujun Zhang,*[,‡] Xian Zhao,[†] Duorong Yuan,*[,†] Chun-Ming Wang,[#] and Thomas R. Shrout[‡]

[†]*State Key Laboratory of Crystal Materials and Institute of Crystal Materials, Shandong University, Jinan 250100, P.R. China,* [‡]*Materials Research Institute, Pennsylvania State University, University Park, Pennsylvania 16802, and* [#]*State Key Laboratory of Crystal Materials and School of Physics, Shandong University, Jinan 250100, P.R. China*

Received December 14, 2009; Revised Manuscript Received February 17, 2010

ABSTRACT: Piezoelectric crystals of neodymium calcium oxyborate, $NdCa_4O(BO_3)_3$ (NdCOB), were grown by the Czochralski technique. The density was measured using the Archimedes method and found to be 3.63 g/cm^3, in good agreement with the theoretical value. The thermal properties of NdCOB have been investigated, with the specific heat being on the order of 0.550 J/(g °C). The four thermal expansion coefficients were measured and found to be $\alpha_{11} = 8.12$, $\alpha_{13} = 0.680$, $\alpha_{22} = 5.96$, and $\alpha_{33} = 10.3$ (10^{-6}/°C), respectively. The relative dielectric permittivities were determined to be $\varepsilon_{11}^T/\varepsilon_0 = 9.90$, $\varepsilon_{22}^T/\varepsilon_0 = 15.5$, $\varepsilon_{33}^T/\varepsilon_0 = 10.2$, and $\varepsilon_{13}^T/\varepsilon_0 = -1.60$, respectively, with corresponding low dielectric loss at 100 kHz, being on the order of <0.1%. The complete set of dielectric, elastic, and piezoelectric constants for NdCOB single crystals were determined by the resonance method and compared to other oxyborate crystals $ReCa_4O(BO_3)_3$ (Re = rare earth), where NdCOB exhibited relatively higher piezoelectric properties with $d_{13} = -4.8$ pC/N, $k_{13} = 16.8\%$, $d_{26} = 16.5$ pC/N, and $k_{26} = 31.1\%$, respectively. The relationship between piezoelectric property and structure was explored, in order to further improve the properties of ReCOB crystals.

1. Introduction

The development of electronic technology toward higher frequency and wider bandwidth has attracted interest in exploring new piezoelectric crystal materials with merits of high thermal stability and large electromechanical coupling factors. Oxyborate crystals $ReCa_4O(BO_3)_3$ (Re = rare earth element, abbreviated as ReCOB) have been studied for nonlinear optical applications, such as second- and third-harmonic generation.[1−8] The crystals can be readily grown from the melt using the Czochralski (CZ) pulling technique at around 1500 °C. The piezoelectric properties, including the surface acoustic wave (SAW) behavior, have been recently investigated.[9−15] $NdCa_4O(BO_3)_3$ (NdCOB) has received attention due to its relatively high SAW coupling factor ($k^2 = 0.8\%$) and low linear temperature coefficient of delay (TCD) (close to zero).[16] Furthermore, NdCOB crystals were found to possess high resistivity, being on the order of 1.2×10^6 Ω·cm at 950 °C, comparable to GdCOB and YCOB,[14,15] together with its good temperature stability of the piezoelectric properties in the temperature range of 20−950 °C, exhibiting the potential use of NdCOB at elevated temperature. Thus, it is desirable to investigate the electrical properties of NdCOB crystals.

To date, some groups have reported the growth of ReCOB crystals,[1,16−19] but papers on the characterization of the piezoelectric properties of NdCOB single crystals are limited. In this work, the CZ growth of NdCOB single crystal was studied. Additionally, the hardness, density, specific heat, and thermal expansion coefficients of NdCOB crystals were determined. Moreover, the full set of dielectric, elastic, piezoelectric, and electromechanical coupling factors of the monoclinic NdCOB were determined. The relationship between piezoelectric property and structure was explored, in order to further improve the properties of ReCOB crystals.

2. Growth of NdCOB Single Crystal

Starting materials for NdCOB crystal growth were high purity (99.99%) $CaCO_3$, Nd_2O_3, and H_3BO_3 powders. They were weighed according to the nominal composition. Considering the evaporation of B_2O_3 during the growth process, an excess of H_3BO_3 (1.0%) was added to the starting materials, in order to obtain good quality crystals with stoichiometric composition. The starting materials were mixed, pressed into tablets, and calcined at 1000 °C for 10 h to decompose H_3BO_3 and $CaCO_3$ completely. After calcinations, the powder was ground, mixed and pressed into pieces, and then sintered at 1100−1200 °C for 10 h to ensure the synthesized polycrystalline NdCOB compound for crystal growth. Crystals were grown by the conventional CZ method in a nitrogen atmosphere containing 4% oxygen by volume. An iridium crucible 60 mm in diameter and 50 mm in height was used and heated by a 2 kHz low radio frequency furnace (TDL-J40 single crystal growth furnace). A special designed after-heater was placed above the crucible to optimize the thermal gradient during the growth. A ⟨010⟩-orientated $YCa_4O(BO_3)_3$ (YCOB) crystal bar was used as a seed to pull the NdCOB crystal from the melt. The pulling rate varied from 1.0 to 3.0 mm/h and the rotation speed was kept between 15 to 20 rpm during the crystal growth. After a final diameter of about 30 mm was reached, the pulling rate was set at 1.0 mm/h with a rotation rate of 16 rpm for the crystal growth. After growth, the crystals were cooled down to room temperature at a rate of 15−35 °C/h.

*Corresponding authors. E-mail: soz1@psu.edu (S.J.Z.); dryuan@sdu.edu.cn (D.R.Y.).

Published on Web 03/08/2010

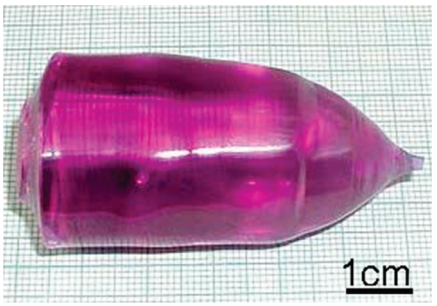

Figure 1. NdCOB single crystal pulled along the *Y*-axis (⟨010⟩ direction).

The as-grown NdCOB crystals were annealed at 1000 °C in air and kept for 20 h, then the crystals were cooled down to room temperature at a rate of 20 °C/h. Figure 1 shows a photograph of an as-grown NdCOB single crystal pulled along the ⟨010⟩ direction, in which the habitual faces ($\bar{2}$01) and (101) can be observed.

3. Experimental Section

The structure and lattice parameters of the as-grown NdCOB crystals were determined by X-ray powder diffraction (XRPD) with a D8 Advance diffractometer (Bruker AXS, Advanced X-ray Solutions) using Cu−Kα radiation (λ = 0.15406 nm) and graphite monochromator at room temperature. The cell parameters were refined and calculated using TREOR 90 software. The mechanical hardness was evaluated for an X-cut NdCOB crystal using an HXS-1000A microhardness tester. The indentation load was 25 g and the selected time was 2 s. The hardness (H_v) and Mohs' hardness values (HM) were calculated using the following relations:

$$H_V = 1.8544\left(\frac{P}{d^2}\right) kg/mm^2$$

and HM = $0.675(H_v)^{1/3}$, respectively.

The crystal density was obtained by two methods. First, the lattice parameters *a*, *b*, and *c* were determined from the powder diffraction. From the lattice parameters and the formula masses of NdCOB, the theoretical density, ρ_x, was calculated using the following equation:

$$\rho_x = \frac{mZ}{abc \sin\beta}$$

where *m* is the molar weight of the crystal, *Z* is the number of molecules in one unit cell, which is two in NdCOB crystal, and *a*, *b*, and *c* are the lattice parameters obtained by the XRPD measurements. For comparison, the experimental density, ρ_e, was determined by the Archimedes method.

Specific heat was measured by differential scanning calorimeter using a simultaneous thermal analyzer (Diamond DSC, Perkin-Elmer) in the temperature range of 20−300 °C, at a constant heating rate of 5 °C /min. The value of the specific heat was calculated by supplied software (Perkin-Elmer Co.). Thermal expansion coefficients of NdCOB crystals were measured in the temperature range from 25 to 500 °C using a thermal dilatometer (Diamond TMA, Perkin-Elmer) at a heating rate of 5 °C /min. For electrical measurements, all the samples were vacuum sputtered with 200 nm platinum thin films on the parallel main faces as the electrodes using a sputter coater (BALTEC SCD 050).

For piezoelectric crystal with space group *Cm*, there are 27 electroelastic constants, including 4 dielectric (ε_{ij}), 10 piezoelectric (d_{ij}), and 13 elastic constants (s_{ij} or c_{ij}). According to the IEEE standard on piezoelectricity,[20] the physical *Y* and *Z* axes are parallel to the crystallographic *b* and *c* axes, respectively, while the *X* axis is perpendicular to the *YZ* plane to form the right-hand orthogonal system. The elastic properties were investigated by the resonance method using an Agilent HP 4294A impedance network analyzer. The dimensions, *t* (thickness) × *w* (width) × *l* (length), were 1.50 × 4.00 × 12.00 mm^3, 1.50 × 8.00 × 8.00 mm^3, and 4.00 × 4.00 × 12.00 mm^3 for bar, plate, and rod samples, respectively.

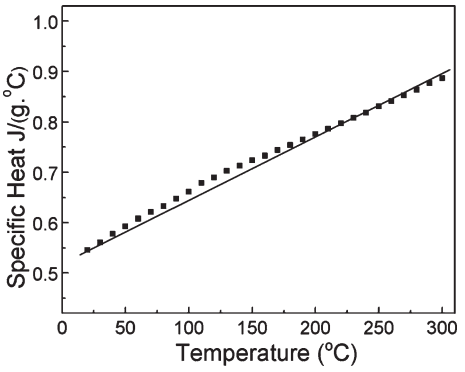

Figure 2. Variation of specific heat with temperature.

4. Results and Discussion

4.1. Hardness and Density. The H_v hardness value determined for ⟨010⟩ oriented samples was found to be 505 kg/mm^2, with Mohs' hardness value being on the order 5.40, comparable to apatite. The X-ray diffraction experiments revealed that NdCOB crystal possessed the space group *Cm*, and the lattice parameters at room temperature were found to be *a* = 0.813, *b* = 1.605, *c* = 0.358 nm, and β = 101.4°, in good agreement with the data of JCPDS No. 50-0399. Using these lattice parameters, the density of the crystal was calculated to be 3.61 g/cm^3. By comparison, the average experimental density was measured and found to be on the order of 3.63 g/cm^3, slightly higher than the theoretical calculated value.

4.2. Specific Heat. The specific heat of the crystalline solids was generally described by the Debye lattice theory in terms of the harmonic frequency spectrum. However, because of the complex structure of NdCOB, it is hard to explain the measured specific heat with the predictions of the lattice theory. The dependence of the specific heat (C_p) of NdCOB with temperature is shown in Figure 2, from which the specific heat value was found to be 0.550 J/(g·°C) at 20 °C, increasing linearly with increasing temperature. The molar mass of NdCOB is 497 g/mol; thus, the C_p of NdCOB was calculated to be 273−442 J/(mol·K), approximate to that of LaCOB.[8]

According to the Law of Dulong & Petit and the Kepp, the atomic energy per mole is $3kTN_A$, where *k* is Boltzmann's constant, *T* is temperature in Kelvins, and N_A is Avogadro's number. Thus, the specific heat can be expressed as

$$C_v = \frac{\partial}{\partial T}(3kTN_A) = 3kN_A/\text{mol} = 24.94 J/(\text{mol}\cdot\text{K}) \quad (1)$$

For NdCOB crystal, there are 18 atoms in one unit cell; thus, the specific heat of NdCOB at 573 K is 449 J/(mol·K), in good agreement with the experimental results. According to the definition of specific heat, the energy change in crystal is related to the variation of temperature and can be expressed as

$$\Delta E = C_V \Delta T \quad (2)$$

where C_V is the specific heat and ΔT the variation of temperature due to thermal absorption by the crystal.[21] From the equation, it can be seen that the temperature gradient is inversely proportional to specific heat, which will induce crystal cracking due to thermal expansion anisotropy. Thus, a large specific heat is desirable for applications at elevated temperature.

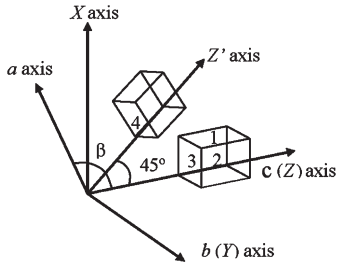

Figure 3. Schematic diagram of the samples for measuring the thermal expansion coefficients.

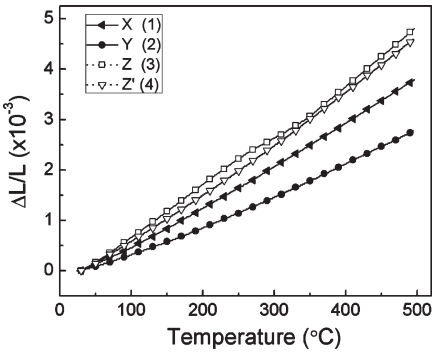

Figure 4. Thermal expansion ratio curves for NdCOB crystals (*X*, *Y*, *Z*, *Z*′ curves correspond to the measured faces 1, 2, 3, and 4 in Figure 3, respectively).

4.3. Thermal Expansion. For a crystal with *Cm* symmetry, there are four independent thermal expansion coefficients (α_{11}, α_{22}, α_{33}, and α_{13}). In the principal coordinate system, the $[\alpha_{ij}]$ tensor is diagonal,

$$\begin{pmatrix} \alpha_{11} & 0 & \alpha_{13} \\ 0 & \alpha_{22} & 0 \\ \alpha_{13} & 0 & \alpha_{33} \end{pmatrix}$$

among which, α_{11}, α_{22}, α_{33} can be obtained by measuring the thermal expansion along *X*-, *Y*-, *Z*-axes, and the measured faces are marked as 1, 2, and 3 in Figure 3, respectively. For α_{13}, rotated *Z*-cut samples (the measured faces are marked as 4 in Figure 3) will be used. For a clockwise rotation of the coordinate axes through an angle θ about the *Y*-axis, the transformation matrix is

$$A_Y = \begin{pmatrix} \cos\theta & 0 & -\sin\theta \\ 0 & 1 & 0 \\ \sin\theta & 0 & \cos\theta \end{pmatrix}$$

Hence, the thermal expansion coefficients $[\alpha_{ij}]$ in the new coordinate system can be written as

$$[\alpha_{ij}]' = A_Y[\alpha_{ij}]A_Y{}^t \quad (3)$$

where the superscript "t" represents "inversion". After rotation, thermal expansion coefficient α_{33} in the new coordinate system becomes

$$\alpha_{33}' = \alpha_{11}\sin^2\theta + 2\alpha_{13}\sin\theta\cos\theta + \alpha_{33}\cos^2\theta \quad (4)$$

from which α_{13} can be easily calculated. Figure 4 presents the thermal expansion curves as a function of temperature for NdCOB. After calculation, the thermal expansion coefficients were determined to be $\alpha_{11} = 8.12$, $\alpha_{22} = 5.96$, $\alpha_{33} = 10.3$, and $\alpha_{13} = 0.680$ (10^{-6}/°C), respectively.

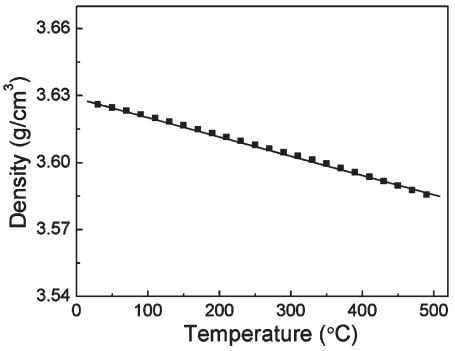

Figure 5. Density variation curves as function of temperature for NdCOB crystals.

4.4. Density versus Temperature Curve. The density temperature coefficient is an important parameter for the determination of zero-temperature-cut orientation. The density temperature equation can be written as

$$\frac{\Delta\rho}{\rho} = \frac{\rho-\rho_0}{\rho_0} = T\rho^{(1)}(\theta-\theta_0) + T\rho^{(2)}(\theta-\theta_0)^2 + T\rho^{(3)}(\theta-\theta_0)^3 \quad (5)$$

where ρ and ρ_0 are the density values at temperatures θ and θ_0, respectively. $T\rho^{(1)}$, $T\rho^{(2)}$, and $T\rho^{(3)}$ are the first-, second-, and third-order density temperature coefficients, respectively. Here, $\theta_0 = 25$ °C is the reference temperature.

The density of NdCOB at different temperatures can be obtained using the following equation:

$$\rho = \frac{m}{abc\sin\beta} = \frac{m}{a_0\left(1+\frac{\Delta a}{a_0}\right)b_0\left(1+\frac{\Delta b}{b_0}\right)c_0\left(1+\frac{\Delta c}{c_0}\right)\sin\beta} = \rho_0\frac{1}{\left(1+\frac{\Delta a}{a_0}\right)\left(1+\frac{\Delta b}{b_0}\right)\left(1+\frac{\Delta c}{c_0}\right)} \quad (6)$$

where $\rho_0 = 3.63$ g cm^{-3} is the measured density of the crystal at $T_0 = 25$ °C, and other values, such as $(\Delta a/a_0)$, $(\Delta b/b_0)$, $(\Delta c/c_0)$, can be obtained from the expansion ratios given in Figure 4. The density versus temperature curve of NdCOB over the temperature range from 25 to 500 °C is given in Figure 5. From the data in Figure 5, density temperature coefficients can be calculated to be $T\rho^{(1)} = -2.26\times10^{-5}$/°C, $T\rho^{(2)} = 1.98\times10^{-9}$/°C, and $T\rho^{(3)} = -1.09\times10^{-11}$/°C, which are comparable to the commercial piezoelectric quartz ($T\rho^{(1)} = -3.49\times10^{-5}$/°C, $T\rho^{(2)} = -1.59\times10^{-8}$/°C, and $T\rho^{(3)} = 5.30\times10^{-12}$/°C).[22]

4.5. Dielectric Properties. The samples (*j*, *g*, *k*, and *l*) shown in Figure 6 were used to determine the dielectric permittivities. Being a second rank tensor, there are four independent dielectric constants similar to the expansion coefficients. Dielectric constants ε_{11}, ε_{22}, ε_{33} can be determined from the capacitances of *X*-, *Y*-, *Z*-cut samples (*k*, *l*, and *j*). For ε_{13} determination, sample (*g*) was used. All the dielectric constants can be obtained directly from the measured capacitance values using the following formulas:

$$\varepsilon_{11,22,33} = \frac{C_{11,22,33}t}{A} \quad (7)$$

$$\varepsilon_{33}' = \varepsilon_{11}\sin^2\theta + 2\varepsilon_{13}\sin\theta\cos\theta + \varepsilon_{33}\cos^2\theta \quad (8)$$

where *C* is the capacitance, *t* is the thickness, *A* is the area of the measured plate, ε_{33}' is the dielectric constant for the

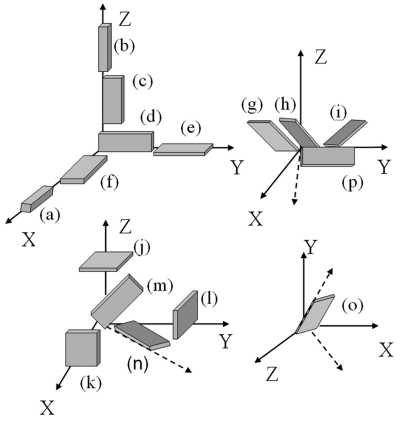

Figure 6. Samples orientation for (a) *X* rod, (b) *Z* rod, (c) *XZ* bar, (d) *XY* bar, (e) *ZY* bar, (f) *ZX* bar, (g) (*XZtwl*) 0°/45°/0° bar, (h) (*XZtwl*) 0°/30°/0° bar, (i) (*XZtwl*)0°/−45°/0° bar, (j) *Z* square plate, (k) *X* square plate, (l) *Y* square plate, (m) (*XYtwl*) 45°/0°/0° bar, (n) (*ZXtwl*)0°/45°/0° bar, (o) (*YZtwl*) 45°/−45°/0° bar, (p) (*ZYtwl*) 0°/0°/45° bar.

Z′-axis (sample g). Here the rotation angle θ is 45°; therefore, ε_{13} can be obtained easily from eq 8. From the equations above, all the relative dielectric permittivities were calculated to be $\varepsilon_{11}^T/\varepsilon_0 = 9.90$, $\varepsilon_{22}^T/\varepsilon_0 = 15.5$, $\varepsilon_{33}^T/\varepsilon_0 = 10.9$, and $\varepsilon_{13}^T/\varepsilon_0 = -1.60$, respectively. The dielectric losses measured at 100 kHz were found to be 0.10%, 0.07%, and 0.09% for *X*-, *Y*-, and *Z*-cut samples, respectively. It is interesting to note that dielectric permittivity $\varepsilon_{13}^T/\varepsilon_0$ is negative, indicating that the dielectric polarization occurs in the negative direction of the *Z*-axis when an electric field is applied along the positive direction of the *X*-axis.[23] According to the energy argument, certain restrictions on the signs and magnitudes of the dielectric permittivities should be followed.[24] The stored electric energy per unit volume must be a positive number; no matter what combination of fields is applied, the energy is greater than zero. Thus, the dielectric permittivities $\varepsilon_{11}^T/\varepsilon_0$, $\varepsilon_{22}^T/\varepsilon_0$, and $\varepsilon_{33}^T/\varepsilon_0$ must be positive. However, off diagonal components, such as $\varepsilon_{13}^T/\varepsilon_0$, are not necessarily positive, but following the relationship $\varepsilon_{11}^T/\varepsilon_0 + \varepsilon_{33}^T/\varepsilon_0 > |2\varepsilon_{13}^T/\varepsilon_0|$, which is the case of the dielectric permittivities in NdCOB crystals.

4.6. Elastic and Piezoelectric Properties. For the determination of the complete set of elastic constants, piezoelectric coefficients and electromechanical coupling factors, samples with different orientations given in Figure 6 were prepared. Piezoelectric strain coefficients d_{11}, d_{33} and elastic compliance constants s_{11} and s_{33} were determined by the resonance technique using eqs 9−11 (samples (a) and (b)). Piezoelectric coefficients d_{13}, d_{12}, d_{32}, and d_{31}, elastic compliance constants s_{33}, s_{22}, and s_{11} were obtained using the eqs 11, 14, and 15 (Samples (c−f)). When measured along the length direction of samples c and f, and along the width direction of the samples d and e, piezoelectric coefficients d_{35}, d_{15}, d_{24}, and d_{26}, and elastic compliance constants s_{55}, s_{44}, and s_{66} could be obtained using eqs 10−13, respectively. Elastic compliance constants, s_{13}, s_{15}, and s_{35}, were determined from transverse length extensional vibration mode of samples (g−i) with the related eqs 14, 16 given below. Similarly, s_{23}, s_{12}, and s_{25} were obtained using eqs 14 and 17−19, corresponding to the samples (m−o). The elastic constant s_{46} was obtained using eqs 13 and 20 by measuring the thickness shear vibration mode of sample (p).

$$s^{\mathrm{E}} = \frac{1}{4\rho l^2 f_{\mathrm{a}}^2 (1-k^2)} \tag{9}$$

$$k^2 = \frac{\pi f_{\mathrm{r}}}{2 f_{\mathrm{a}}} \cot \frac{\pi}{2}\left(\frac{f_{\mathrm{r}}}{f_{\mathrm{a}}}\right) \tag{10}$$

$$d = k(\varepsilon s)^{1/2} \tag{11}$$

$$s^{\mathrm{E}} = \frac{1}{4\rho w^2 f_{\mathrm{a}}^2 (1-k^2)} \tag{12}$$

$$s^{\mathrm{E}} = \frac{1}{4\rho t^2 f_{\mathrm{a}}^2 (1-k^2)} \tag{13}$$

$$s^{\mathrm{E}} = \frac{1}{4\rho l^2 f_{\mathrm{r}}^2} \tag{14}$$

$$\frac{k^2}{1-k^2} = \frac{\pi f_{\mathrm{a}}}{2 f_{\mathrm{r}}} \cot \frac{\pi}{2}\left(\frac{f_r}{f_a}\right) \tag{15}$$

$$s_{33}'(XZtwl/0^{\mathrm{o}}/\theta/0^{\mathrm{o}}) = s_{11}\sin^4\theta + (2s_{13} + s_{55})\sin^2\theta\cos^2\theta + 2s_{15}\sin^3\theta\cos\theta + s_{33}\cos^4\theta + 2s_{35}\sin\theta\cos^3\theta \tag{16}$$

$$s_{22}'(XYtwl/45^{\mathrm{o}}/0^{\mathrm{o}}/0^{\mathrm{o}}) = (s_{22} + 2s_{23} + s_{44} + s_{33})/4 \tag{17}$$

$$s_{11}'(ZXtwl/45^{\mathrm{o}}/0^{\mathrm{o}}/0^{\mathrm{o}}) = (s_{11} + 2s_{12} + s_{66} + s_{22})/4 \tag{18}$$

$$s_{33}'(YZtwl/45^{\mathrm{o}}/-45^{\mathrm{o}}/0^{\mathrm{o}}) = (4s_{22} + s_{11} + s_{33} + 2s_{15} + 2s_{13} + s_{55} + 2s_{35} + 4s_{23} + 4s_{12} + 4s_{25} + 2s_{44} + 2s_{66} + 4s_{46})/16 \tag{19}$$

$$s_{44}'(XYtwl/0^{\mathrm{o}}/0^{\mathrm{o}}/45^{\mathrm{o}}) = s_{44}/2 + s_{46} + s_{66}/2 \tag{20}$$

$$d_{13}'(XZtwl/0^{\mathrm{o}}/\theta/0^{\mathrm{o}}) = d_{11}\sin^2\theta\cos\theta - d_{31}\sin^3\theta + d_{13}\cos^3\theta - d_{33}\sin\theta\cos^2\theta + d_{15}\sin\theta\cos^2\theta - d_{35}\sin^2\theta\cos\theta \tag{21}$$

$$d_{13}'(XZtwl/0^{\mathrm{o}}/45/0^{\mathrm{o}}) + d_{13}'(XZtwl/0^{\mathrm{o}}/-45/0^{\mathrm{o}}) = \sqrt{2}/2(d_{11} + d_{13} - d_{35}) \tag{22}$$

$$d_{33}'(YZtwl/0^{\mathrm{o}}/\theta/0^{\mathrm{o}}) = d_{11}\sin^3\theta + d_{31}\sin^2\theta\cos\theta + d_{13}\cos^2\theta\sin\theta + d_{33}\cos^3\theta + d_{15}\sin^2\theta\cos\theta + d_{35}\cos^2\theta\sin\theta \tag{23}$$

$$d_{33}'(YZtwl/0^{o}/30/0^{o}) + d_{33}'(YZtwl/0^{o}/-30/0^{o}) = \sqrt{3}/4(d_{31} + 3d_{33} + d_{15}) \tag{24}$$

For confirming the sign and magnitude of the piezoelectric coefficient d_{15}, extra samples (g) and (i) were evaluated using the related eqs 21 and 22. For checking the sign of d_{35}, additional samples geometry of rods (*YZtwl*)0/θ/0 (θ = 30° and −30°) were characterized using eqs 23 and 24. On the basis of the measurements and calculations

Table 1. Dielectric, Elastic, and Piezoelectric Properties of NdCOB, YCOB, GdCOB, and LaCOB Crystals[a]

Elastic Compliance Constants s^{E}_{ij} (pm^2/N)

	s_{11}	s_{12}	s_{13}	s_{15}	s_{22}	s_{23}	s_{25}	s_{33}	s_{35}	s_{44}	s_{46}	s_{55}	s_{66}
NdCOB	8.3	−1.4	−3.7	2.0	7.4	−0.7	1.8	9.4	−0.4	30.9	0.3	22.4	20.5
NdCOB[a]	8.3	−2.0	−3.5	−0.9	7.5	−1.6	0.5	9.4	0.9	34.0	1.0	22.0	20.0
YCOB[b]	7.15	−0.35	−2.8	0.74	6.91	−0.68	−0.46	8.79	−1.2	35.0	3.5	23.0	15.0
GdCOB[b]	7.6	−1.2	−3.9	0.4	7.15	−4.6	−1.5	8.94	0.32	28.0	1.7	23.0	18.0
GdCOB[c]	7.6	−0.92	−0.95	−0.99	7.1	−0.92	−14	8.9	−0.33	17.0	14.0	19.0	18.0
LaCOB[b]	8.82	−1.1	−2.6	1.1	4.78	−1.2	3.4	10.1	−1.3	34.0	1.3	19.0	18.0

Relative Dielectric Permittivities ε^{T}_{ij}

	ε_{11}	ε_{13}	ε_{22}	ε_{33}
NdCOB	9.90	−1.60	15.5	10.2
NdCOB[a]	9.90	−0.80	15.0	10.0
YCOB[b]	9.57	−0.96	11.4	9.52
GdCOB[b]	10.5	0.8	14.0	10.4
GdCOB[c]	9.03	0.75	12.35	10.25
LaCOB[b]	9.87	1.2	14.3	9.87
LaCOB[d]	9.87	−1.24	14.9	9.87

Piezoelectric Strain Constants d_{ij} (pC/N)

	d_{11}	d_{12}	d_{13}	d_{15}	d_{24}	d_{26}	d_{31}	d_{32}	d_{33}	d_{35}
NdCOB	2.7	4.1	−4.8	3.0	4.5	16.5	−1.9	−3.7	2.1	2.3
NdCOB[a]	1.7	3.9	−4.9				−1.4	−2.5	1.5	
YCOB[b]	1.4	3.8	−4.2	−7.2	−2.6	8	−0.22	−2.3	0.83	2.2
GdCOB[b]	2.8	4.8	−3.8	−6.9	0.45	11	−0.77	−2.4	2.5	−4
GdCOB[c]	2.4	4.0	−4.5	0.66	−2.8	2.4	−1.1	−2.2	2.0	−2.7
LaCOB[b]	2.1	3.9	−3.9				−0.55	−2.2	1.5	
LaCOB[d]	1.28	3.89	−3.89	0.62	6.41	8.73	−0.55	−2.22	1.10	

Electromechanical Coupling Coefficients k_{ij} (%)

	k_{11}	k_{12}	k_{13}	k_{15}	k_{24}	k_{26}	k_{31}	k_{32}	k_{33}	k_{35}
NdCOB	10.1	16.2	16.8	6.8	7.0	31.1	7.1	14.4	7.3	5.2
NdCOB[a]		15.4	16.8				4.7	9.4		

[a] Data (a) is from ref 25, data (b) is from ref 26, data (c) is from ref 13, and data (d) is from ref 23.

above, all the dielectric, elastic, and piezoelectric constants can be achieved.

Table 1 lists the full set of constants for NdCOB and compared to the reported values for YCOB, GdCOB, and LaCOB single crystals. The piezoelectric coefficients of NdCOB crystals ($d_{13} = -4.8$ pC/N, $d_{24} = 4.5$ pC/N, and $d_{26} = 16.5$ pC/N) were found to be larger than those of YCOB, GdCOB, and LaCOB crystals. Of particular interest is the high shear electromechanical coupling factor k_{26}, being on the order of 31.1%.

Figure 7 shows the piezoelectric coefficient d_{26} as a function of rare earth (Re) cation radius for different ReCOB crystals, using data collected from the literature (YCOB, GdCOB, and LaCOB).[23,26] It can be found that the piezoelectric coefficient d_{26} increased with increasing Re ion radius from Y ($r^{Y}(+3) = 0.90$ Å) to Nd ($r^{Nd}(+3) = 0.983$ Å), with the exception of LaCOB ($r^{La}(+3) = 1.032$ Å), where d_{26} was found to decrease. A similar phenomenon was reported by Nakao et al,[16] but no explanation was given. It is believed that the piezoelectric coefficient d_{26} may be affected by the following two factors:

(1) The radius of Re ions. A large ion radius gives rise to a large Re−O bond length and lattice parameters a and c, enlarging the volume of the Re−O oxygen octahedron (see Figure 8). However, the Re−O bond length cannot be increased limitlessly with increasing Re^{3+} ion radius, as the ratio of the Re−O bond length to Re^{3+} ion radius may be decreased (high ratio indicates the large space between the two ions), which can affect the extent of lattice distortion, thus resulting in a small magnitude of s_6 strain developed by an applied field E_2 along the crystallographic b-axis (physical Y-axis); hence, d_{26} is decreased.

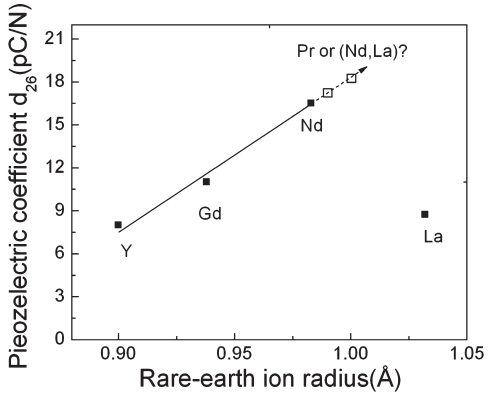

Figure 7. Piezoelectric coefficients d_{26} versus rare-earth ion radius.

(2) Distribution of cations in crystals and disorder structure. The ion radius of Ca^{2+} is 1.00 Å, larger than the rare-earth ion radius of Nd ($r^{Nd}(+3) = 0.983$ Å), Y ($r^{Y}(+3) = 0.90$ Å) and Gd ($r^{Gd}(+3) = 0.938$ Å), while smaller than that of La($r^{La}(+3) = 1.032$ Å).[27] Iliukhin et al reported disorder in the distribution of Ca and Gd ions (0.86Gd and 0.14 Ca on the Gd sites) with respect to their theoretical sites in GdCOB crystal.[28] It is possible for Re^{3+} ions to occupy the sites of Ca1(4b), and for Ca^{2+} to be on the sites of Re1(2a) in ReCOB crystals, especially in the case of

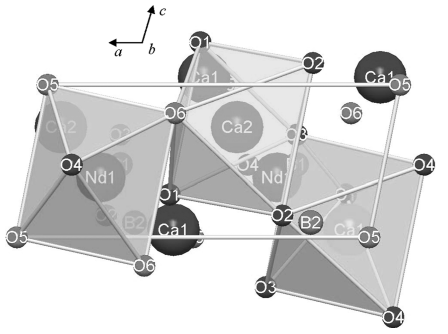

Figure 8. Crystal structure of NdCOB (observed along the crystallographic *b* axis).

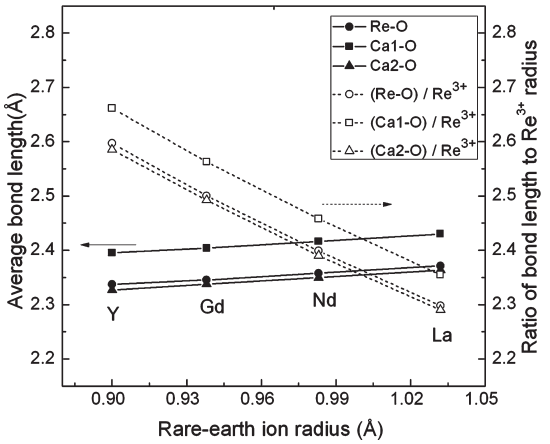

Figure 9. Average bond length versus Re^{3+} ion radius.

NdCOB, due to their similar ion radius, giving rise to the disordered structure. From the data given in the PDF Cards (LaCOB: PDF Card, 04-009-2918; NdCOB: PDF Card, 04-009-2919; GdCOB: PDF Card, 04-009-2920; YCOB: PDF Card, 04-009-2921), it is clear that the average bond length of Ca1−O is longer than that of Re−O in the octahedrons. Thus, when Re^{3+} occupies a larger octahedron, the octahedron will be distorted and generate a larger magnitude of s_6 strain when an applied field E_2 along the crystallographic *b*-axis, improving the piezoelectric coefficient d_{26}. For La^{3+} and Y^{3+}, however, the ion radius is very different from that of Ca^{2+}, so it is hard for them to occupy the sites of Ca1(4b); in this case, factor (1) becomes dominant.

Figure 9 presents the average bond lengths of Re1−O, Ca1−O, and Ca2−O versus Re^{3+} ion radius. It can be found that the average bond length of Re1−O, Ca1−O, and Ca2−O increased simultaneously with increasing ion radius. However, the ratio of average bond length to ion radius was found to decrease sharply with the increasing of the Re^{3+} ion radius, indicating the effective space distance gets short and the extent of lattice distortion weakens, which may lead to the decrease of the d_{26}.

Table 2 presents the lattice parameters and cation radius of various oxyborate crystals. On the basis of the results in Figures 7 and 9 and Table 2, the high piezoelectric d_{26} in NdCOB crystal can be attributed to the following reasons: (1) the large ion radius results in a large Re−O bond length and lattice parameters *a* and *c*; (2) the radius of Nd^{3+} (0.983 Å) is similar to that of Ca^{2+} (1.00 Å), so it is easy for Nd^{3+} to occupy Ca1−O octahedron while Ca^{2+} can occupy Nd−O octahedron, leading to a disordered structure. Both of the above will be in favor of octahedron distortion and results in a large magnitude of strain s_6 when electric field E_2 is applied along the crystallographic *b*-axis, which gives rise to improved d_{26} values. According to the above two assumptions, it is expected that the $(Nd,La)Ca_4O(BO_3)_3$ [(Nd,La)COB] and/or $PrCa_4O(BO_3)_3$ [PrCOB] crystal(s) will possess higher d_{26} values, due to the ion radius of Pr^{3+} being on the order of ~0.990 Å and is located between Nd^{3+} and La^{3+} ions, whereas the average ion radius of the complex ion $(Nd,La)^{3+}$ can be tuned to be ~1.000 Å by adjusting the Nd/La ratio. The exploration of the new (Nd,La)COB and PrCOB crystals are now under way.

Table 2. Lattice Parameters and Rare-Earth Ion Radius of Various Oxyborate Crystals

	lattice parameters and ion radius					
oxyborate crystals	*a* (Å)	*b* (Å)	*c* (Å)	*β*	V (Å)^3	$r^{Re}(+3)$ (Å)
YCOB	8.077	16.02	3.534	101.19	448.01	0.900
LaCOB	8.172	16.08	3.629	101.43	467.41	1.032
NdCOB	8.145	16.06	3.607	101.37	459.85	0.983
GdCOB	8.104	16.03	3.558	101.25	453.38	0.938

5. Conclusions

NdCOB single crystals were grown by the Czochralski pulling method. The measured density was found to be 3.63 g/cm^3, in good agreement with the theoretical value. The density temperature coefficients were found to be $T\rho^{(1)} = -2.26 \times 10^{-5}$/°C, $T\rho^{(2)} = 1.98 \times 10^{-9}$/°C, and $T\rho^{(3)} = -1.09 \times 10^{-11}$/°C, respectively. The specific heat of NdCOB was 0.550 J/(g·°C) at room temperature, and the thermal expansion coefficients were calculated to be $\alpha_{11} = 8.12$, $\alpha_{13} = 0.680$, $\alpha_{22} = 5.96$, and $\alpha_{33} = 10.3$ (10^{-6}/°C), respectively. The relative dielectric permittivities were found to be $\varepsilon_{11}^T/\varepsilon_0 = 9.90$, $\varepsilon_{22}^T/\varepsilon_0 = 15.5$, $\varepsilon_{33}^T/\varepsilon_0 = 10.2$, and $\varepsilon_{13}^T/\varepsilon_0 = -1.60$, with the dielectric loss being on the order of < 1.0% at 100 kHz, which is very important for SAW devices application. The full tensor matrix of the dielectric, electromechanical, piezoelectric, and elastic constants of the NdCOB has been measured. NdCOB crystals were found to possess relatively higher values of piezoelectric properties with $d_{13} = -4.8$ pC/N, $k_{13} = 16.8\%$, $d_{26} = 16.5$ pC/N, and $k_{26} = 31.1\%$, respectively, when compared to other ReCOB crystals, indicating that NdCOB is a promising candidate for piezoelectric applications. New crystals (Nd,La)COB and PrCOB are now being investigated, in order to further improve the piezoelectric coefficients.

Acknowledgment. The author (F. P. Yu) wishes to thank the support from China Scholarship Council and Prof. X. Yin for discussion. This work supported by NSF under Grant No. ECCS09-25586.

References

(1) Fei, Y. T.; Chai, B. H. T.; Ebbers, C. A.; Liao, Z. M.; Schaffers, K. I.; Thelin, P. *J. Cryst. Growth* **2006**, *290*, 301–306.
(2) Zhang, S. J.; Zhang, J. G.; Cheng, Z. X.; Zhou, G. Y.; Han, J. R.; Chen, H. C. *J. Cryst. Growth* **1999**, *203*, 168–172.
(3) Aka, G.; Salin, F.; Pelenc, D. J. *Opt. Soc. Am. B* **1997**, *14*, 2238–2247.
(4) Ge, W. W.; Zhang, H. J.; Wang, J. Y.; Jiang, M. H.; Sun, S. Q.; Ran, D. G.; Xia, H. R.; Boughton, R. I. J. *Appl. Crystallogr.* **2007**, *40*, 125–132.
(5) Zhang, S. J.; Cheng, Z. X.; Lu, J. H.; Li, G. M.; Lu, J. R.; Shao, Z. S.; Chen, H. C. *J. Cryst. Growth* **1999**, *205*, 453–456.

(6) Zhang, S. J.; Cheng, Z. X.; Zhang, S. J; Han, J. R.; Sun, L. K.; Chen, H. C. *J. Cryst. Growth* **2000**, *213*, 415–418.
(7) Ye, Q; Chai, B. H. T. *J. Cryst. Growth* **1999**, *197*, 228–235.
(8) Zhang, H. J.; Jiang, H. D.; Wang, J. Y.; Hu, X. B.; Yu, G. W.; Yu, W. T.; Gao, L; Liu, J. A.; Zhang, S. J.; Jiang, M. H. *Appl. Phys. A: Mater. Sci. Process.* **2004**, *78*, 889–893.
(9) Wang, J.; Hu, X.; Yin, X.; Song, R.; Wei, J.; Shao, Z.; Liu, Y.; Jiang, M.; Tian, Y.; Jiang, J.; Huang, W. *J. Mater. Res.* **2001**, *16*, 790–796.
(10) Takeda, H.; Sako, H.; Shimizu, H.; Kodama, K.; Nishida, M.; Nakao, H.; Nishida, T.; Okamura, S.; Shikida, T.; Jpn., J. *Appl. Phys. Part 1* **2003**, *42*, 6081–6085.
(11) Shimizu, H.; Nishida, T.; Nishida, M.; Takeda, H.; Shiosaki, T.; Jpn., J *Appl. Phys. Part 1* **2005**, *44*, 7059–7063.
(12) Zhang, S. J.; Fei, Y. T.; Frantz, E.; Synder, D. W.; Chai, B. H. T.; Shrout, T. R. *IEEE Trans. Ultrason. Ferroelect. Frequency Control* **2008**, *55*, 2703–2709.
(13) Pawlaczyk, C.; Markiewicz, E.; Klos, A.; Hofman, W.; Pajaczkowska, A. *Phys. Status Solidi A* **2006**, *203*, 2103–2118.
(14) Zhang, S. J.; Fei, Y. T.; Chai, B. H.T.; Frantz, E.; Snyder, D. W.; Jiang, X. N.; Shrout, T. R. *Appl. Phys. Lett.* **2008**, *92*, 202905.
(15) Zhang, S.; Frantz, E.; Xia, R.; Everson, W.; Randi, J.; Snyder, D. W.; Shrout, T. R. *J. Appl. Phys.* **2008**, *104*, 084103.
(16) Nakao, H.; Nishida, M.; Shikida, T.; Shimizu, H.; Takeda, H.; Shiosaki, T. J. *Alloys Compd.* **2006**, *408*, 582–585.
(17) Furuya, H.; Yoshimura, M.; Kobayashi, T.; Murase, K.; Mori, Y.; Sasaki, T. *J. Cryst. Growth* **1999**, *198/199*, 560–563.
(18) Vivien, D.; Aka, G.; Kahn-harari, A.; Aron, A.; Mougel, F.; Bénitez, J.; et al. *J. Cryst. Growth* **2002**, *237*, 621–628.
(19) Mougel, F.; Kahn-Harari, A.; Aka, G.; Pelenc, D. *J. Mater. Chem.* **1998**, *8*, 1619–1623.
(20) *IEEE Standard on Piezoelectricity. An American National Standard*; IEEE: New York, **1987**; Vol. *14*.
(21) Kachhava C. M. *Solid State Physics*; McGraw-Hill: New Delhi, 1990.
(22) Zhang P. L.; Zhong W. L. *Physics of Piezoelectric Materials and Devices*; Shandong Science & Technology Press: Shangdong, 2000; p 112.
(23) Shimizu, H.; Kodama, K.; Takeda, H.; Nishida, T.; Shikida, T.; Okamura, O.; Shiosaki, T. *Jpn J. Appl. Phys.* **2004**, *43*, 6716–6720.
(24) Newnham R. E. *Properties of Materials: Anisotropy, Symmetry, Structure*; Oxford University Press: Oxford, 2005; pp 60−62.
(25) Karaki, T.; Adachi, M.; Kuniyoshi, Y. *J. Electroceram.* **2008**, *21*, 823–826.
(26) Shimizu, H.; Nishida, T.; Takeda, H.; Shiosaki, T. *J. Cryst. Growth* **2009**, *311*, 916–920.
(27) Shannon, R. D. *Acta Crystallogr. Sect. A: Cryst. Phys., Theor., Gen. Crystallogr.* **1976**, *32*, 751–767.
(28) Ilyukhin, A. B.; Dzhurinskii, B. F. *Russ. J. Inorg. Chem.* **1993**, *38*, 917–920.